PHYSICAL REVIEW B VOLUME 57, NUMBER 21 1 JUNE 1998-I

Thermochemical reduction of yttria-stabilized-zirconia crystals: Optical and electron microscopy

B. Savoini, C. Ballesteros, J. E. Muñoz Santiuste, and R. González
Escuela Politécnica Superior, Universidad Carlos III de Madrid, Butarque 15, Leganés E-28911, Madrid, Spain

Y. Chen
Division of Materials Sciences, Office of Basic Energy Sciences, U.S. Department of Energy, ER 131, Germantown, Maryland 20874-1290

(Received 2 December 1997)

Thermochemical reduction (TCR) at high temperatures has been performed on yttria-stabilized zirconia (YSZ), undoped and doped with Ni:Er, Co, or Pr. Investigations were carried out using optical absorption, luminescence, and analytical electron microscopy. After TCR, undoped crystals show an extinction band centered at about 1.8 eV which is attributed to Mie scattering from precipitates with an average size of 10 nm, as observed by analytical transmission electron microscopy. In crystals codoped with Ni:Er, TCR induced a broad extinction band centered at 1.3 eV beginning at 1600 K. Metallic Ni colloids contributing to Mie scattering have an average size of 100 nm. Similarly, in Co-doped crystals a broad band at 0.9 eV, emerging at 1750 K, was attributed to metallic colloids observed to have an average dimension of 200 nm. In all cases, the precipitate distribution is very inhomogeneous. These results agree qualitatively with the predictions of the Mie theory for the extinction bands associated with metal colloids embedded in the matrix. Electron microscope observations indicate that the degradation of the optical properties experienced by previously reduced YSZ crystals during oxidation at elevated temperatures is a bulk effect probably related to cavities and dislocations. [S0163-1829(98)01421-0]

I. INTRODUCTION

Zirconia (ZrO_2) has three polymorphs: the monoclinic, tetragonal, and cubic structures. The monoclinic phase is stable up to about 1373 K, where it transforms to the tetragonal phase; at about 2643 K the crystal adopts the cubic fluorite structure. At room temperature, only the monoclinic form is stable. Addition of heterovalent cations (mainly Ca^{2+} and Y^{3+}) stabilizes the cubic polymorph. Cubic yttria stabilized zirconia (YSZ) is an ionic conductor over a wide range of oxygen partial pressures at elevated temperatures. This ionic conduction occurs via oxygen-ion hoppings through anion vacancies created to preserve electrical neutrality when Y^{3+} is added.[1]

Undoped YSZ single crystals are transparent in the as-grown state. After either thermochemical reduction (TCR) (Refs. 2–6) or electroreduction [2,6] they become colored. Optical absorption measurements in the former show[5,6] that (1) the absorption edge shifts towards higher energies, (2) a strong broad band centered at 2.64 eV (470) nm, (3) a shoulder peaking at 3.3 eV (375) nm, and (4) a weak band at 1.8 eV (700) nm. These absorption bands have previously been assigned to electrons trapped at oxygen vacancies nearest to Zr cations and to oxygen ions with trapped holes adjacent to yttria cations.[5] The brown coloration induced by TCR was not observed in Pr^{3+}-doped yttria stabilized zirconia reduced at temperatures as high as 1873 K.[6,7] In general, it is found that TCR at sufficiently high temperatures causes precipitation of metal impurities which results in broad extinction bands attributed to Mie scattering from precipitates.[8–16] Even in undoped oxide crystals, precipitation of inherently present impurities, such as iron, was observed.[13,14] A necessary condition for the colloid formation is the presence of a high concentration of oxygen vacancies. Therefore TCR creates precipitates by increasing vacancy concentrations. The vacancies first associate themselves with impurity ions and then cluster to form precipitates, therefore, impurity precipitates should not be uncommon. Nevertheless, with the exception of ZrN precipitates in cubic zirconia deformed in compression in argon at elevated temperatures,[17] identification of impurity precipitates has not been reported in YSZ.

In this paper, optical absorption and analytical transmission electron microscopy (TEM) have been used to characterize defects in YSZ crystals, both undoped and doped with different impurities (Ni-Er, Co, and Pr) before and after TCR. Nickel or cobalt doped crystals were chosen because precipitation of both ions was previously observed in other oxides and the precipitates were well characterized.[9–12,16] Metallic colloids are also identified in YSZ. The conditions for colloid formation and thermal stability are investigated. Oxidation of TCR crystals produces a degradation of their optical properties; the crystal becomes translucent and exhibits a white coloration. Oxidized crystals were also investigated by scanning electron microscopy (SEM).

II. EXPERIMENTAL PROCEDURE

Single crystals of ZrO_2 stabilized with 16 wt. % of Y_2O_3 were purchased from CERES Corporation (USA). In this investigation, undoped crystals and those doped with Ni:Er, Co, and Pr, grown by the skull method were used.

Samples were cut with a diamond saw and polished to optical quality. Powder x-ray diffraction patterns of the samples were recorded with an X'Pert-MPD Philips diffractometer using Cu K_α radiation. X-ray analysis shows that these crystals have a well crystallized cubic fluorite structure

TABLE I. Chemical analyses of undoped and doped YSZ crystals.

Element	YSZ (ppm)	YSZ: Ni: Er (ppm)	YSZ: Co (ppm)	YSZ:Pr (ppm)
Bi	194	329	1361	205
Ca	1301	<1136	1760	1949
Ce	448	<435	<380	0
Co	0	0	1021	<505
Cu	<299	<374	<298	<305
Er	<409	7365	<430	0
Fe	424	492	514	588
Hf	10286	9738	9421	8765
K	2081	3009	5212	2684
Mn	0	<268	<234	<274
Nd	<324	<335	<291	0
Ni	262	473	299	262
Pr	<425	<438	<382	743
Y	216 903	204 130	198 804	191 740
Zn	0	0	0	1492
Zr	766 643	771 476	779 592	790 487

with a lattice parameter of 0.5146 nm, in agreement with previously reported values.[18]

TCR was performed by placing the samples inside a graphite container surrounded by flowing oxygen-free nitrogen gas inserted in a horizontal furnace. High-temperature oxidizing treatments were made in flowing oxygen gas.

Optical absorption measurements in the UV-VIS-IR were made with a Perkin-Elmer Lambda 19. Infrared absorption data were taken with a Perkin-Elmer 2000 FT-IR. For high resolution emission measurements a Spectra Physics Ar^+ laser was used as the excitation source. The emitted light was focused into the entrance slit of a SPEX 1000M monochromator and detected with a Hamamatsu R943-02 cooled photomultiplier. The spectra were recorded with a Sr400 gated photon counter or a HP7240 nanovoltmeter.

For transmission electron microscopy, specimens were first cut into discs of 3 mm and then dimpled to a thickness below 30 μm and argon milled in a liquid-nitrogen-cooled holder with an acceleration voltage of 5 kV and an incidence angle of 15°. TEM x-ray microanalysis and electron diffraction studies of the individual precipitates were carried out with a JEOL 2000 FX, a JEOL 2000 FX II, and a Philips CM200 field emission analytical electron microscope operated at 200 kV. The latter one was equipped with a beryllium specimen holder. Scanning electron microscopy was performed with a Philips XL30 scanning electron microscope. The samples were coated with a thin conducting layer of carbon to remove surface charge.

III. EXPERIMENTAL RESULTS

A. Chemical analysis

X-ray fluorescence analyses were made on undoped YSZ crystals and on crystals with the dopants Ni:Er, Co, and Pr. The impurity analysis is given in Table I. All crystals inadvertently contain iron and copper.

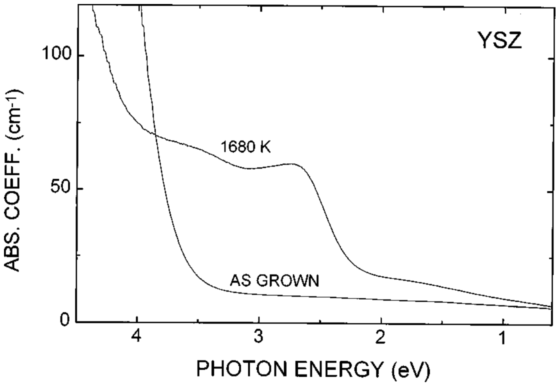

FIG. 1. Optical absorption spectra of an undoped YSZ crystal before and after TCR at 1680 K for 15 min.

B. Optical absorption and extinction measurements

Thermochemical reduction of YSZ crystals results in changes in the optical absorption spectra. These changes are associated with different types of defects. Broad extinction bands have been related in different oxides to Mie scattering from precipitates generated during the TCR process. We characterized the optical spectra before and after TCR for undoped and doped crystals.

Undoped YSZ crystals. The optical absorption spectra of a nominally undoped YSZ sample before and after TCR are shown in Fig. 1. In reduced crystals, the absorption edge shifts towards higher energies and a strong composed band appears at 2.64 eV (470 nm) with a full width at half maximum (FWHM) of about 0.5 eV. This band can be decomposed in two bands peaking at 2.6 and 2.7 eV.[5] This composed band is responsible for the brown coloration of the crystals. In addition, two less intense bands are observed at 3.3 eV (375 nm) and 1.8 eV (688 nm). Previously, these absorption bands have been tentatively[5] assigned to electrons trapped at oxygen vacancies nearest to Zr cations in trigonal (3.3 eV band) or cubal (2.6 and 1.8 eV) symmetries and to oxygen ions with trapped holes adjacent to yttria cations (2.7 eV).

The 1.8 eV band is very broad with a FWHM of 1.2 eV. The FWHM of this magnitude is more consistent with extinction from precipitates than from electronic transitions. Indeed, TEM observations show that small precipitates are present in reduced crystals (Sec. III D 1). The formation of this band was investigated by reducing a YSZ crystal for 15 min at increasing temperatures with increments of 50 K. The increase in extinction coefficient at 1.8 eV versus temperature is plotted as curve A in Fig. 2. A threshold temperature for the band formation was found to be ≈1425 K. The thermal stability of this band, using a sample previously reduced at 1673 K for 15 min, is demonstrated in Fig. 3. The sample was isochronally annealed for 15 min interval in flowing oxygen. After the anneal at 1100 K, the band at 2.64 eV has significantly decreased (Fig. 3). This different behavior suggests that both bands may have a different origin. At ≈1173 K, before the loss of the extinction at 1.8 eV starts to occur, the sample begins to turn white and becomes translucent. A broad band covering the visible spectrum and extending into the infrared region emerges (Fig. 3). After the anneal at 1373 K, the sample became completely white and the 1.8 and 2.64

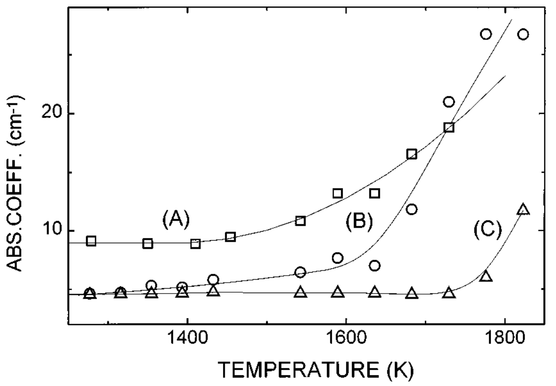

FIG. 2. Absorption coefficient versus temperature after isochronal anneals: (a) 1.8 eV band in undoped YSZ crystals, (b) 1.3 eV band in YSZ:Ni:Er, and (c) 0.9 eV band in YSZ:Co. The points of curve A are displaced upward to avoid overlapping of the three curves.

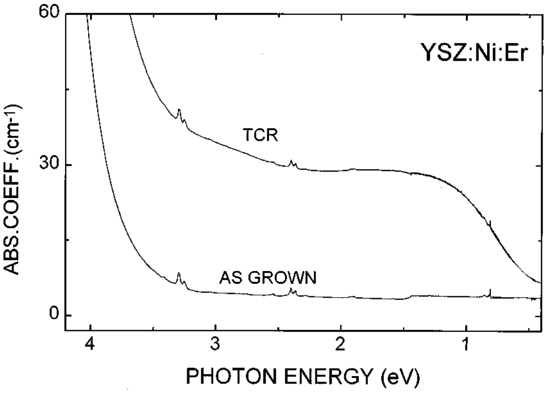

FIG. 4. Optical absorption spectra of a YSZ:Ni:Er crystal before and after TCR at 1823 K for 1 h.

eV bands could not be distinguished. The sample degradation will be characterized by TEM and SEM in Secs. III D 2 and III D 3.

YSZ:Ni:Er. The absorption spectrum of an as-grown YSZ crystal codoped with Ni and Er is shown in Fig. 4. Five groups of narrow absorption bands at about 3.29, 2.40, 1.89, 1.58, and 0.81 eV associated to Er^{3+} are apparent.[19] Nickel-absorption bands are expected to appear at 2.9 and 2.4 eV (Refs. 20,21) but are hardly visible because the nickel concentration was too low. After TCR at 1823 K for 1 h, the Er^{3+} absorption bands and the same broad band at 3.3 eV observed in reduced undoped crystals are present. The intensity of the Er^{3+} bands remains almost unchanged (Fig. 4). In addition, a broad extinction covering the visible spectrum and extending into the infrared region appears. As a result the samples acquire a dark coloration. This band is centered in the vicinity of 1.3 eV with a FWHM of about 1.2 eV. Earlier studies have shown that TCR on nickel-doped MgO or Al_2O_3 crystals resulted in broad extinction bands which were due to Mie scattering from nickel metallic precipitates, with extinction bands centered at about 2.2 and 2.1 eV, respectively.[9–11,16] In the following section, we will provide evidence that the dark coloration is due to Mie scattering from Ni-rich precipitates.

Optical absorption measurements were used to monitor the presence of nickel colloids. One sample was subjected to isochronal TCR treatments from 1273 to 1823 K for 15 min each. Selected optical spectra are shown in Fig. 5. The lowest curve represents a virgin crystal. The broad band at 3.3 eV appeared after 1450 K. The broad band at 1.3 eV also seemed to grow with temperature. The enormously large FWHM indicates that it too is due to Mie scattering from colloids. The increase in extinction coefficient at 1.3 eV is plotted as a function of the incubating temperature as curve B in Fig. 2. A threshold temperature was about 1600 K.

Isochronal annealing in flowing oxygen was performed on a sample previously reduced at 1573 K for 75 min (Fig. 6). Two observations were noted: (a) loss of the extinction band at 1.3 eV began to occur at ≈1200 K, and (b) the sample became translucent and turned white. After annealing at 1373 K, the sample turned completely white and the stability of the colloid band at 1.3 eV could not be discerned.

YSZ:Co. Thermochemical reduction was performed on a YSZ:Co sample at 1823 K for 1 h. Figure 7 shows the spectra before and after TCR. In the as-grown crystal, the $d \rightarrow d$ transitions of Co^{2+} ions are apparent in the visible region (also see inset in Fig. 7).[21,22] After TCR, the two bands at 3.3 and 2.64 eV present in thermochemically reduced undoped crystals are also observed. In addition, a broad extinction band (FWHM=1.2 eV) in the infrared is observed at ≈0.9 eV (Fig. 7). The Co^{2+} intensities have decreased, indicating that some Co^{2+} ions have precipitated. The band at 0.9 eV is attributed to the Co colloid. The amount of cobalt colloids was monitored by optical absorption measurements. One

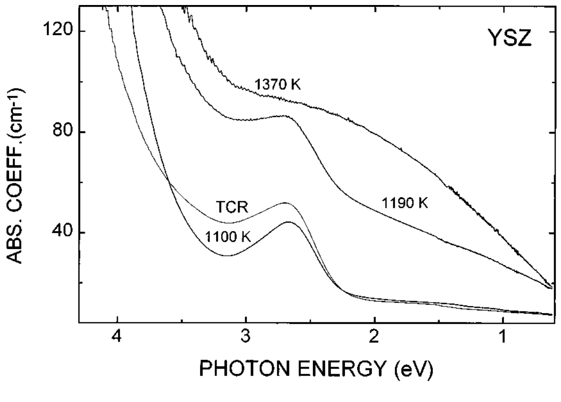

FIG. 3. Optical absorption spectra of an undoped YSZ crystal after TCR and subsequent anneals in flowing oxygen at increasingly higher temperatures.

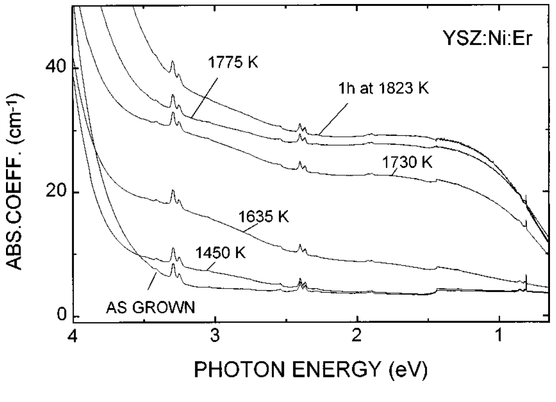

FIG. 5. Optical absorption spectra of a YSZ:Ni:Er crystal before and after TCR at increasingly higher temperatures.

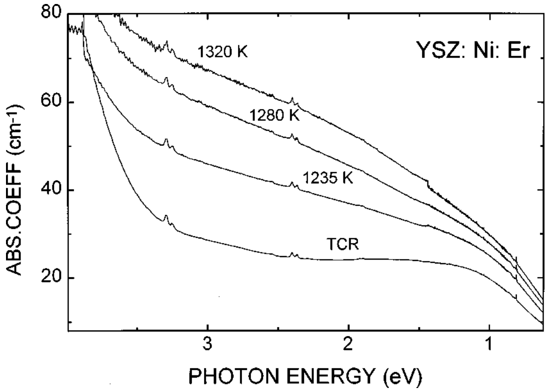

FIG. 6. Optical absorption spectra of a YSZ:Ni:Er crystal before and after TCR and subsequent anneals in flowing oxygen at increasingly higher temperatures.

sample was reduced isochronally at increasing temperatures between 1273 and 1823 K for 15 min each. The increase in absorption coefficient at 0.9 eV is plotted as a function of the incubating temperature as curve C in Fig. 2. The threshold temperature was ≈ 1750 K. The thermal stability of the precipitates could not be determined because of the sample degradation in oxidizing atmospheres already mentioned for undoped crystals and YSZ:Ni:Er. TEM characterization of cobalt precipitates will be performed in Sec. III D 1.

YSZ:Pr. TCR was performed on a Pr-doped crystal at 1600 K for 30 min. The spectra before and after TCR are shown in Fig. 8. In thermochemically reduced crystals neither the brown coloration nor absorption edge shift is observed. Only the absorption band at 3.3 and the extinction at 1.8 eV are present. The Pr^{3+} absorption coefficients (not shown in the figure) do not significantly change with TCR. The presence of the broad band centered at about 1.8 eV without the 2.64 band indicates that the two bands do not necessarily have the same origin and gives further support to the previously mentioned idea that the former band is associated to extinction from precipitates.

C. Lifetime luminescence measurements

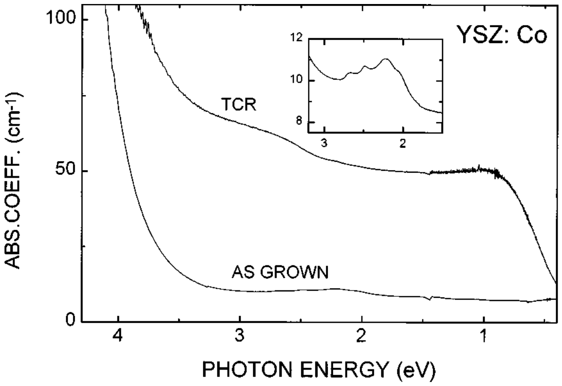

FIG. 7. Optical absorption spectra of a YSZ:Co crystal before and after TCR at 1823 K for 1 h.

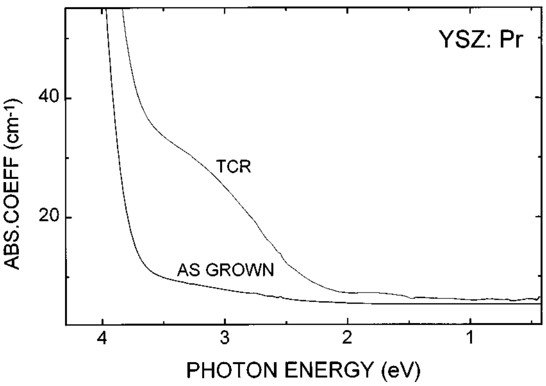

FIG. 8. Optical absorption spectra of a YSZ:Pr crystal before and after TCR at 1600 K for 30 min.

Large ions such as Er and Pr are not expected to precipitate at temperatures of ≈1800 K. Indeed, confirmation was provided by TEM (next section). The lifetime of the Pr^{3+} luminescence critically depends on the distances among Pr^{3+} ions dispersed in the matrix. Therefore it provides information on Pr^{3+} ion association and possible changes in local concentration. Lifetime luminescence experiments were performed in YSZ:Pr crystals, before and after TCR, to determine any concentration change experienced by the praseodymium substitutional impurity during TCR. They were excited at 2.7 eV. The decay of the induced luminescence at 2.0 eV was recorded before and after TCR. Nearly exponential decays were found with lifetime values of (177 ±10) and (162±15) μs, respectively. The lifetime did not significantly change. These results indicate that the concentration of the substitutional praseodymium dispersed in the matrix remained practically constant, hence neither praseodymium precipitates nor very small praseodymium clusters are expected to be formed in significant amounts during TCR.

D. Transmission electron microscopy

Optical absorption and luminescence experiments indicated that TCR selectively causes precipitates in crystals doped with lighter impurities, such as in Ni:Er or Co. Transmission electron microscopy observations were performed

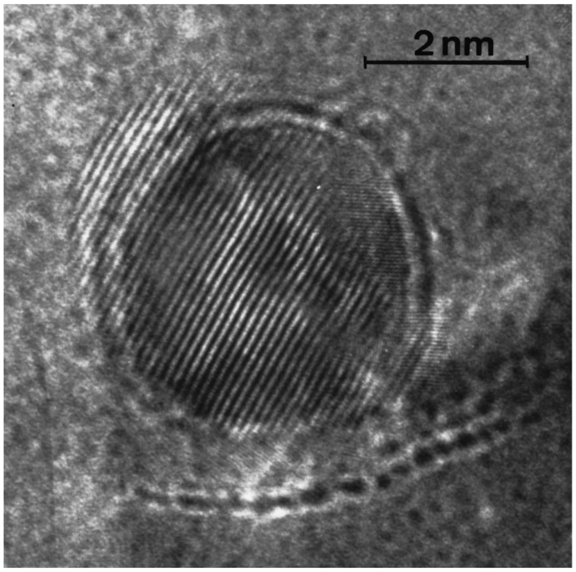

FIG. 9. Micrograph of a copper-rich precipitate showing moiré and lattice fringes.

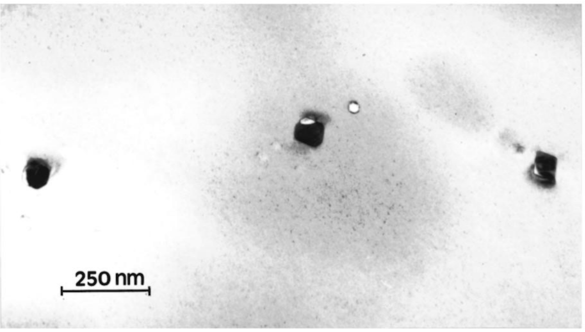

FIG. 10. Transmission electron micrograph showing the Ni precipitates in a YSZ:Ni:Er specimen.

for verification. Also, undoped crystals were studied to determine whether inherently present impurities form precipitates and whether the 1.8 eV band is related to these precipitates. In general, precipitates were not found in as-grown YSZ crystals, either doped or undoped. On the other hand, TCR crystals contain precipitates which were inhomogeneously distributed. Areas with a high concentration of precipitates were separated by regions which were almost free from precipitates. In addition, dislocation, dislocation loops, and voids were imaged.

1. Precipitates

YSZ undoped crystals. After TCR, small precipitates with an average size of ≈10 nm were imaged. Figure 9 shows a precipitate imaged under multibeam conditions. Moiré and lattice fringes could be observed. X-ray microanalysis using the small convergent probe show that the precipitates are rich in copper. These observations indicate that the 1.8 eV band observed in the absorption spectra could be due to Mie scattering from Cu-rich precipitates.

YSZ:Ni:Er. Figure 10 shows an electron micrograph from a region containing precipitates in a TCR Ni:Er-doped YSZ specimen. The black spots are due to precipitates. The average size was determined to be 100 nm. High magnification micrographs showed that the shape of the precipitates was not always well defined (Fig. 11). Also, voids are often observed near or associated with the precipitates.

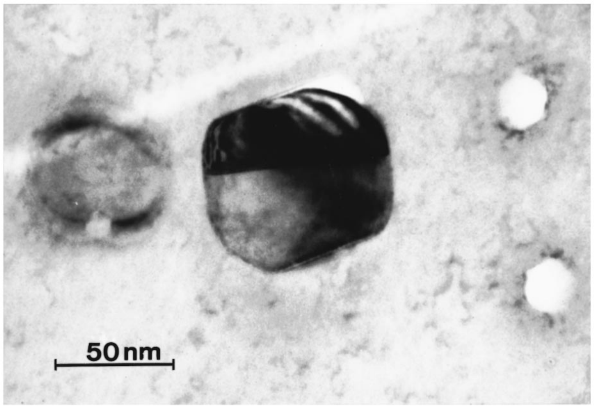

FIG. 11. Transmission electron micrograph of a Ni precipitate with a poorly defined shape in a YSZ:Ni:Er specimen. On the right side two voids are also observed.

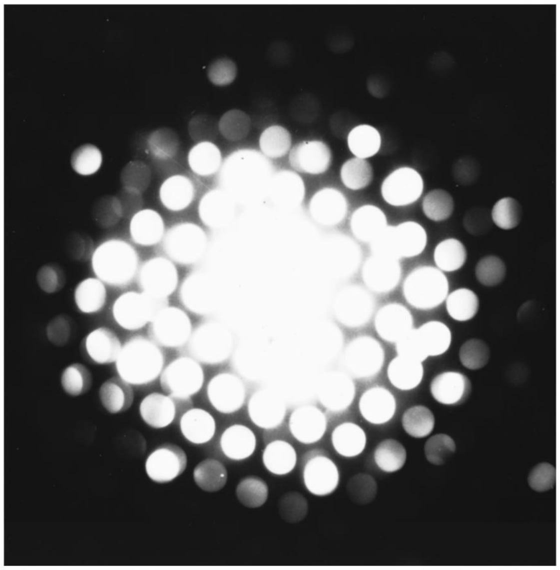

FIG. 12. Microdiffraction pattern from a fcc nickel precipitate in a YSZ:Ni:Er specimen.

The structure of the precipitates was investigated by microdiffraction techniques. Figure 12 shows a microdiffraction pattern obtained from a precipitate embedded in the matrix. It therefore contained matrix as well as precipitate reflections. Using the YSZ matrix spots as an internal calibration, the precipitate reflections were found to correspond to a fcc crystal structure with a lattice constant of $a_0 = 3.55$ Å, which suggests bulk fcc nickel. Microdiffraction patterns also showed that the precipitates were incoherent.

X-ray microanalysis was also performed on precipitates. Figure 13 shows a typical x-ray fluorescence spectrum exhibiting a NiK_α line at 7.47 keV, a NiK_β line at 8.26 keV, and a NiL line at 0.85 keV. TCR of the YSZ system containing both a small ion (Ni) and a large ion (Er) results only in precipitation of the lighter ions.

YSZ:Co. Electron microscopy studies of YSZ:Co crystals after TCR showed the presence of precipitates. These precipitates had an average size of about 200 nm (Fig. 14). Microdiffraction patterns indicate that the reflections associated with the precipitates correspond to a fcc cobalt in the β

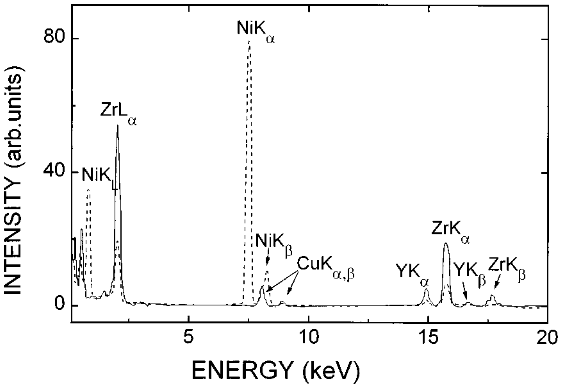

FIG. 13. Energy-dispersive x-ray fluorescence spectrum from a Ni precipitate showing the Ni K_α, Ni K_β, and Ni L lines (dotted line) and from the matrix (solid line). The $\mathrm{Cu}_{\alpha,\beta}$ lines are produced at the microscope specimen holder.

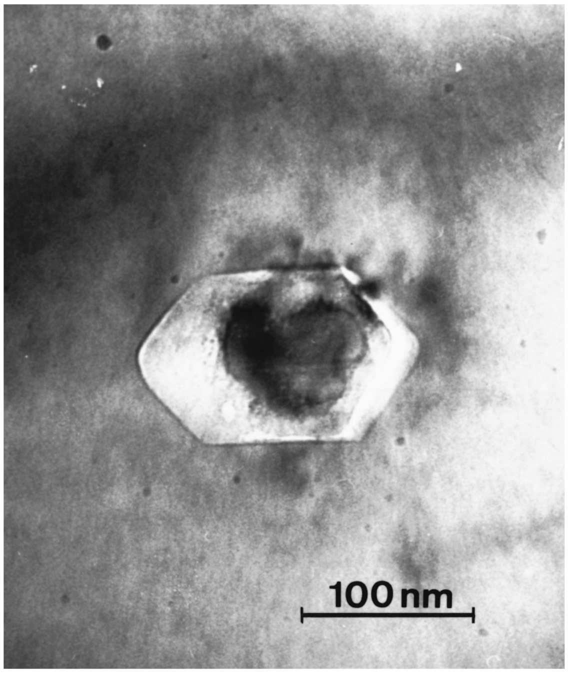

FIG. 14. High magnification transmission electron micrograph showing a Co precipitate in a YSZ:Co specimen.

phase with a lattice constant of 3.56 Å; the precipitates were incoherent (Fig. 15). X-ray microanalysis identified cobalt as the precipitates. Figure 16 shows a typical x-ray fluorescence spectrum exhibiting a CoK_α line at 6.93 keV and Co K_β line at 7.65 keV.

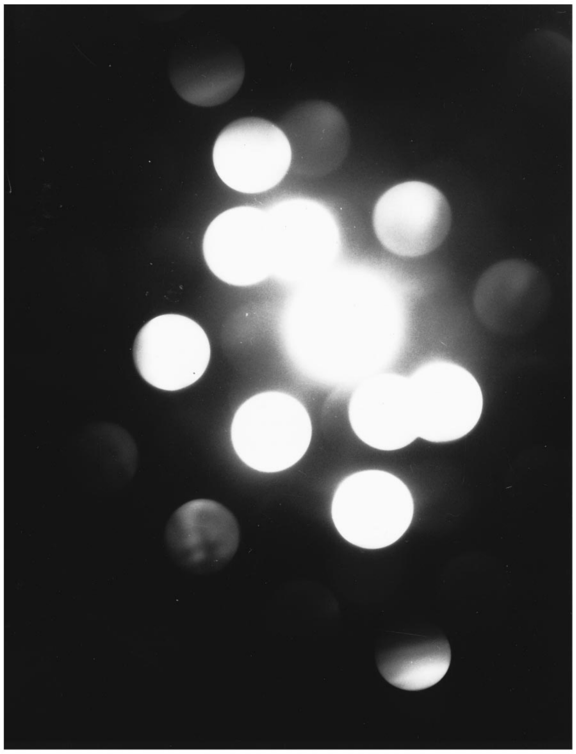

FIG. 15. Microdiffraction pattern from a fcc cobalt precipitate in a YSZ:Co specimen.

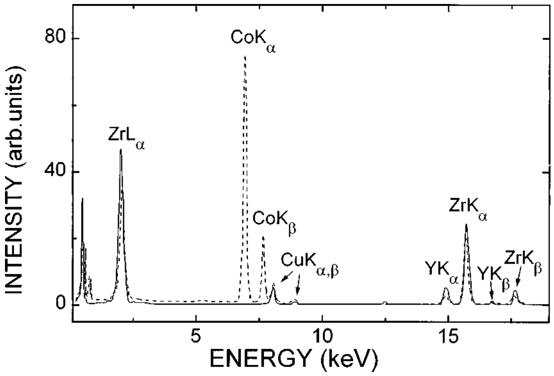

FIG. 16. Energy-dispersive x-ray fluorescence spectrum from a Co precipitate showing the Co K_α and Co K_β lines (dotted line) and from the matrix (solid line). The Cu$_{\alpha,\beta}$ lines are produced at the microscope specimen holder.

2. Cavities and dislocations

Electron microscopy observations indicated that in all the specimens which were thermochemically reduced, voids are inhomogeneously distributed. The presence of precipitates was attended by dislocations and cavities. As indicated earlier, oxidation of TCR crystals induces translucency which at higher temperatures becomes opaque white. TEM revealed that the translucency is attended by cavities whose concentration increases dramatically at oxidization temperatures above 1273 K. Figure 17 shows a micrograph illustrating both cavities and dislocations. In oxidized samples the size and concentration of precipitates is much smaller, as expected. Electron diffraction patterns indicated that after oxidation of a previously reduced crystal, the crystalline structure of the sample is still cubic fluorite with a lattice constant in agreement with the 0.5146 nm value determined by x-ray diffraction patterns in as-grown crystals. The translucency induced by the oxidation is attributed to cavities, and to changes at the sample surface.

3. Surface characterization

To characterize the region near the crystal surface, scanning electron microscopy was performed in as-grown, reduced, and subsequently oxidized samples. The operating electron energy was 15 keV. The samples were imaged in the

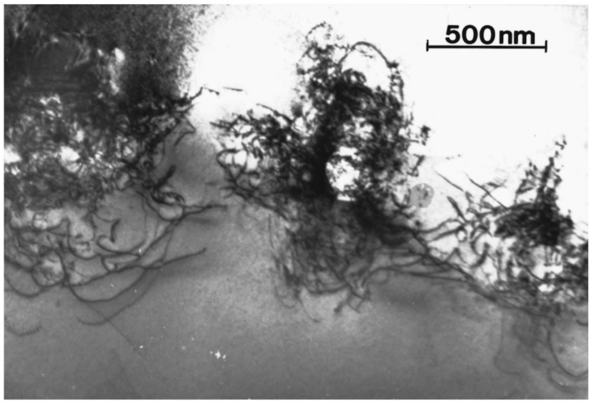

FIG. 17. Transmission electron micrograph showing cavities and dislocations in a YSZ:Ni:Er specimen after TCR and subsequent oxidation.

emissive electron mode, that is, with secondary and backscattered electrons. Figure 18(a) illustrates a micrograph of an as-grown crystal. The crystal surface appears smooth; the only remarkable features are the straight lines running across the surface. These lines are scratches produced during the mechanical polishing with emery paper. After TCR at 1823 K for 15 min, the sample surface appears dramatically degraded: a high density of cavities was observed, mainly following the polishing scratching lines [Fig. 18(b)]. After oxidation at 1373 K for 15 min, regions with a granular morphology appeared; the particle size was of the order of 4 μm [Fig. 18(c)]. When the crystals were abraded to remove the surface region and polished to optical quality, the sample exhibits long fracture lines and a high density of homogeneously distributed small cracks separated by smooth surface regions [Fig. 18(d)]. The smooth regions increase in size as the surface removal progresses and the concentration of surface cracks decreased; however, the cracks did not disappear. The polished sample does not recover its transparency and still looks white. The same results were obtained for doped crystals.

IV. DISCUSSION AND CONCLUSIONS

According to the Mie theory,[23,24] the extinction coefficient due to a dilute concentration N of spherical particles of radius R and volume V embedded in a dielectric medium with a homogeneous distribution is given by

$$\gamma=\frac{6\pi NV}{\lambda'}\mathrm{Im}\sum_{\nu=1}^{\infty}(-1)^{\nu}\left(\frac{a_{\nu}-p_{\nu}}{2\alpha^{3}}\right), \tag{1}$$

where λ' is the wavelength of the light in the matrix and $\alpha=2\pi(R/\lambda')$. The quantities a and p are the electric and magnetic multipoles of order ν which are functions of the colloid radii and of the dielectric constant of both the particles and the matrix.

For small colloids ($R<10$ nm), using only the first term in Eq. (1), the extinction maximum occurs at a wavelength λ given by

$$\lambda_m=\frac{2\pi c}{\omega_p}(\epsilon_0+2m_0^2). \tag{2}$$

Here c is the vacuum speed of light, ω_p the plasma frequency of the metal, $\epsilon_0\approx 1$ the static dielectric constant of the metal, and m_0^2 the real part of the dielectric constant of the matrix.

Equation (2) indicates that the position of the maximum is independent of the colloid radius, and for colloids made of different metals in the same matrix, depends only on the plasma frequency. For nickel and cobalt precipitates, these frequencies are almost identical: $\omega_p(\mathrm{Ni})=2.410\times10^{16}\ \mathrm{s}^{-1}$ and $\omega_p(\mathrm{Co})=2.406\times10^{16}\ \mathrm{s}^{-1}$. Therefore, the extinction bands due to nickel and cobalt precipitates should peak at nearly the same wavelength. Using the same argument, the extinction band due to copper precipitates should peak at longer wavelengths, because $\omega_p(\mathrm{Cu})=1.642\times10^{16}\ \mathrm{s}^{-1}$.

Obviously, our experimental findings do not agree with predictions from Eq. (2). This disagreement is not surprising; this equation is not valid for large colloids ($R>10$ nm)

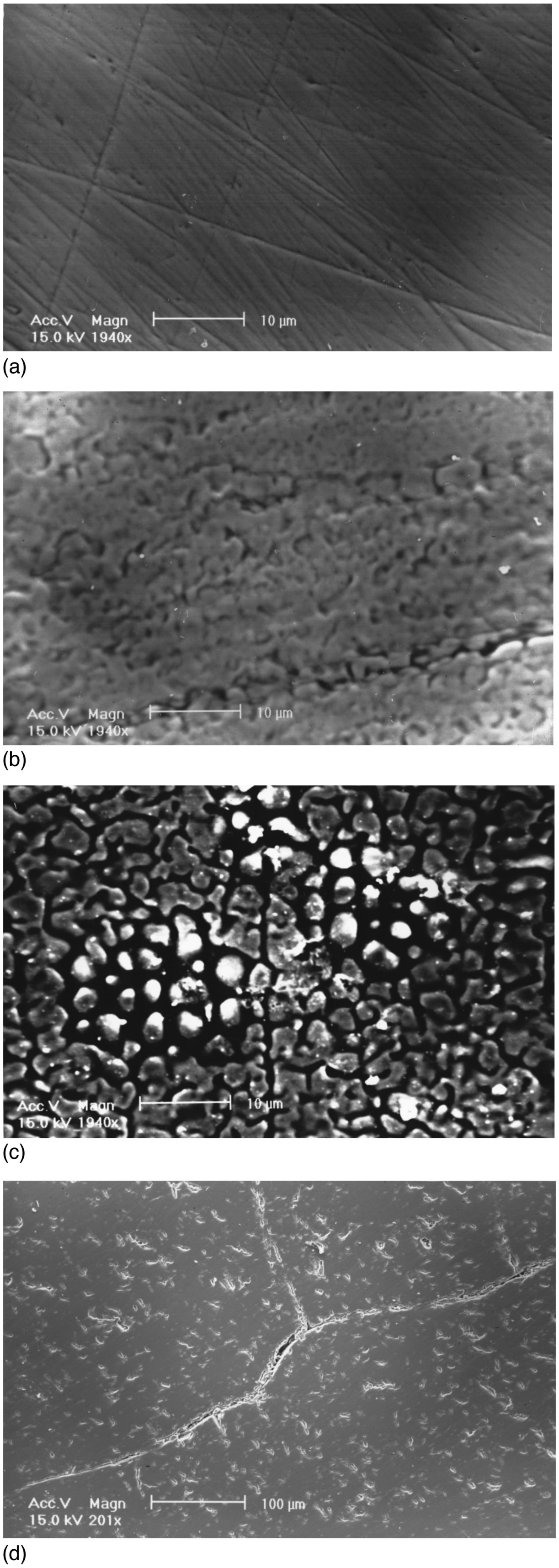

FIG. 18. Scanning electron microscope images in the emissive mode for an undoped YSZ sample: (a) as-grown, (b) after TCR at 1823 K for 15 min, (c) subsequent oxidation at 1373 K for 15 min, and (d) abrasion with emery paper.

which is the present situation. Extinction bands have been calculated as a function of R, by using higher terms in the Mie Eq. (1).[24–28] The main features are (1) the band half-width and peak wavelength are functions of R, the type of metal and the host crystal, (2) as R increases, the bands become broader and move to longer wavelengths. Since nickel and cobalt have almost the same plasma frequency, the peak wavelength is determined by the precipitate size. Experimentally we observed that (a) the dimensions were $\approx$100 and 200 nm for the nickel and cobalt precipitates, respectively, and (b) the corresponding extinction band peaks occurred at 1.3 and 0.9 eV, in qualitative agreement with the theory. For copper precipitates, the situation is not as straightforward. The plasma frequency effect would shift the maximum towards longer wavelengths relative to that of nickel colloids, but the size effect (10 compared to 100 nm) would shift the peak to shorter wavelengths. We previously attributed the extinction band at 1.8 eV to copper colloids. This would indicate that size effect dominates in this case.

It should also be noted that in MgO single crystals, the nickel and cobalt precipitates have been shown to have an average size of about 50 and 100 nm, respectively, and the corresponding extinction bands are centered at about 2.2 and 3.7 eV.[10,12] The location of the nickel and cobalt extinction bands occurs at shorter wavelengths than in YSZ because (1) according to Eq. (2), the position of the band maximum moves towards higher wavelengths as the real part of the dielectric constant m_0^2 of the matrix increases; for MgO and YSZ, m_0^2 is $\approx$3.0 and $\approx$4.8, respectively. (2) The sizes of both Ni and Co precipitates are smaller by a factor of 2 in MgO than in YSZ. However, MgO crystals do not satisfy the assertion that the larger the precipitate size, the shorter the wavelength of the peak band position. Our observations indicate that the results of the application of the Mie theory to the study of the extinction bands due to large colloids in oxides are only partially valid, probably due to deviation effects from the spherical shape, precipitate size distribution, and inhomogeneous distribution of the precipitates.

We shall now address the ability of various impurity ions to aggregate and form precipitates. To begin with, we know from x-ray fluorescence analyses (Table I) that YSZ crystals, including those nominally pure, contain large amounts of different impurities besides those intentionally introduced during crystal growth; in particular, the iron concentration is of the order of 500 cationic ppm. After TCR at 1823 K only Ni, Co, or Cu-rich precipitates were identified. No Fe precipitates were observed. In contrast, in two other systems, MgO and MgAl$_2$O$_4$, iron precipitates were formed during TCR at $\approx$ 2000 K, even though the Fe content was significantly smaller.[13,14] These observations raise the question of why impurities, such as Fe, do not form precipitates in YSZ. The answer could be ionic radii. For Cu^{2+}, Ni^{2+}, Co^{2+}, and Fe^{2+} the radii are 0.69, 0.72, 0.74, and 0.76 Å, respectively. For precipitates to be created, the impurity ions need to diffuse and aggregate with oxygen vacancies. The smaller the ionic radius, the lower the diffusion temperature. This is indeed the case for Ni^{2+} and Co^{2+} ions for which the threshold temperatures for forming precipitates were 1600 and 1750 K, respectively; the higher Co concentration apparently did not lower the threshold temperature sufficiently. The threshold formation for the 1.8 eV band, which we attribute to copper precipitates, was $\approx$1425 K. Iron precipitates were not observed, presumably because the temperature was not sufficiently high; 1850 K was the maximum capability of our furnace. Precipitation of larger ions, radii such as Er^{3+} (0.96 Å) and Pr^{3+}(1.09 Å) require even higher temperatures. Indeed, luminescence lifetime experiments in Pr-doped crystals show no evidence of Pr precipitation during TCR, indicating again that the mobility of a large ion such as Pr^{3+} is very low at 1800 K.

TEM indicates that the translucency and opaque white developed during oxidation of TCR crystals is a bulk effect associated with the buildup of cavities. No phase transition has been observed.

ACKNOWLEDGMENTS

This work has been supported by the Comisión Asesora de Investigación Científica y Técnica of the Spanish Government and the Comunidad Autónoma de Madrid (CAM). TEM observations were made in the Centro de Microscopía Luis Brú and in the Instituto de Materiales (CSIC). We are indebted to P. Herrero, J. González, and A. Muñoz for their assistance with the TEM and SEM observations.

---

[1] W. D. Kingery, J. Pappis, M. E. Doty, and D. C. Hill, J. Am. Ceram. Soc. **42**, 393 (1959).

[2] D. A. Wright, J. S. Thorp, A. Aypar, and H. P. Buckley, J. Mater. Sci. **8**, 876 (1973).

[3] E. D. Wachsman, N. Jiang, C. W. Frank, D. M. Mason, and D. A. Stevenson, Appl. Phys. A: Solids Surf. **50**, 545 (1990).

[4] V. R. PailVerneker, A. N. Petelin, F. J. Crowne, and D. C. Nagle, Phys. Rev. B **40**, 8555 (1989).

[5] V. M. Orera, R. I. Merino, Y. Chen, R. Cases, and P. J. Alonso, Phys. Rev. B **42**, 9782 (1990).

[6] B. Savoini, J. E. Muñoz-Santiuste, R. González, and Y. Chen, J. Lumin. **72-74**, 714 (1997).

[7] B. Savoini, J. E. Muñoz-Santiuste, and R. González, Phys. Rev. B **56**, 5856 (1997).

[8] S. C. Jain, N. D. Arora, and K. L. Chaudhary, J. Appl. Phys. **45**, 2368 (1974).

[9] J. Narayan, Y. Chen, and R. M. Moon, Phys. Rev. Lett. **46**, 1491 (1981).

[10] J. Narayan, Y. Chen, R. M. Moon, and R. N. Carpenter, Philos. Mag. A **49**, 287 (1984).

[11] R. M. Bunch, W. P. Unruh, and M. V. Iverson, J. Appl. Phys. **58**, 1474 (1985).

[12] C. Ballesteros, R. González, and Y. Chen, Phys. Rev. B **37**, 8008 (1988).

[13] C. Ballesteros, R. González, S. J. Pennycook, and Y. Chen, Phys. Rev. B **38**, 4231 (1988).

[14] C. Ballesteros, L. S. Cain, S. J. Pennycook, R. Gonzĺez, and Y. Chen, Philos. Mag. A **59**, 907 (1989).

[15] C. Ballesteros, R. González, Y. Chen, and M. R. Kokta, Phys. Rev. B **47**, 2460 (1993).

[16] C. Ballesteros, Yi Chen, Y. Chen R. González, M. R. Kokta, and X. F. Zong, Philos. Mag. A **76**, 357 (1997).

[17] D. Gómez-García, J. Martínez-Fernández, A. Domínguez-Rodriguez, and K. Westmacott, J. Am. Ceram. Soc. **79**, 487 (1996).

[18] T. H. Etsell and S. N. Flengas, Chem. Rev. **70**, 339 (1970).

[19] R. I. Merino, V. M. Orera, R. Cases, and M. A. Chamarro, J. Phys.: Condens. Matter **3**, 8491 (1991).

[20] B. Savoini, J. E. Muñoz-Santiuste, and R. González (unpublished).

[21] M. Kunz, H. Kretschmann, W. Assmus, and C. Klingshirn, J. Lumin. **37**, 123 (1987).

[22] V. M. Orera, R Merino, R. Cases, and R. Alcalá, J. Phys.: Condens. Matter **5**, 3717 (1993).

[23] G. Mie, Ann. Phys. (Leipzig) **25**, 377 (1908).

[24] A. E. Hughes and S. C. Jain, Adv. Phys. **28**, 717 (1979), and references therein.

[25] J. H. Schulman and W. D. Compton, *Color Centers in Solids* (Pergamon Press, Oxford, 1962).

[26] D. C. Skilman and C. R. Berry, J. Chem. Phys. **48**, 3297 (1968).

[27] S. C. Jain and N. D. Arora, J. Phys. Chem. Solids **35**, 1231 (1974).

[28] R. Fuchs, Phys. Rev. B **11**, 1732 (1975).